RESEARCH ARTICLE

3D Printing of Tricalcium Phosphate/Poly Lactic-co-glycolic Acid Scaffolds Loaded with Carfilzomib for Treating Critical-sized Rabbit Radial Bone Defects

Ye Li[1†], Kegong Xie[1†], Chong Wang[2†], Chengliang Yang[1], Ke Huang[1], Feng Li[1], Chuanchuan Zheng[1], Jian Chen[1], Shujun Dong[3], Guangfeng Deng[4], Gege Huang[4], Qiaoyan Lu[4], Jia Liu[1*], Kai Li[5*], Yujin Tang[1*], Liqiang Wang[6]

[1]Department of Orthopaedics, Affiliated Hospital of Youjiang Medical University for Nationalities, Baise, Guangxi, PR China
[2]School of Mechanical Engineering, Dongguan University of Technology, Songshan Lake, Dongguan, Guangdong, PR China
[3]Department of Rehabilitation medicine, Affiliated Hospital of Youjiang Medical University for Nationalities, Baise, Guangxi, PR China
[4]Youjiang Medical University for Nationalities, Baise, Guangxi, PR China
[5]The Third Affiliated Hospital of Southern Medical University, Guangzhou, Guangdong, PR China
[6]State Key Laboratory of Metal Matrix Composites, School of Material Science and Engineering, Shanghai Jiao Tong University, Shanghai, 200240, China
[†]*These authors contributed equally to this work*

Abstract: The rapid development of scaffold-based bone tissue engineering strongly relies on the fabrication of advanced scaffolds and the use of newly discovered functional drugs. As the creation of new drugs and their clinical approval often cost a long time and billions of U.S. dollars, producing scaffolds loaded with repositioned conventional drugs whose biosafety has been verified clinically to treat critical-sized bone defect has gained increasing attention. Carfilzomib (CFZ), an approved clinical proteasome inhibitor with a much fewer side effects, is used to replace bortezomib to treat multiple myeloma. It is also reported that CFZ could enhance the activity of alkaline phosphatase and increase the expression of osteogenic transcription factors. With the above consideration, in this study, a porous CFZ/β-tricalcium phosphate/poly lactic-co-glycolic acid scaffold (designated as "cytidine triphosphate [CTP]") was produced through cryogenic three-dimensional (3D) printing. The hierarchically porous CTP scaffolds were mechanically similar to human cancellous bone and can provide a sustained CFZ release. The implantation of CTP scaffolds into critical-sized rabbit radius bone defects improved the growth of new blood vessels and significantly promoted new bone formation. To the best of our knowledge, this is the first work that shows that CFZ-loaded scaffolds could treat nonunion of bone defect by promoting osteogenesis and angiogenesis while inhibiting osteoclastogenesis, through the activation of the Wnt/β-catenin signaling. Our results suggest that the loading of repositioned drugs with effective osteogenesis capability in advanced bone tissue engineering scaffold is a promising way to treat critical-sized defects of a long bone.

Keywords: Bone defect; Cryogenic 3D printing; Bone regeneration; β-tricalcium phosphate; Carfilzomib

*Correspondence to: Jia Liu, Department of Orthopedics, Affiliated Hospital of Youjiang Medical University for Nationalities, Baise, Guangxi, 533000, China: liujia0111@live.cn; Kai Li, The Third Affiliated Hospital of Southern Medical University, Guangzhou, Guangdong Province, 510000, China: lk516433415@smu.edu.cn; Yujin Tang, Department of Orthopedics, Affiliated Hospital of Youjiang Medical University for Nationalities, Baise, Guangxi, 533000, China: tangyujin1967@163.com

Received: July 12, 2021; **Accepted:** August 2, 2021; **Published Online:** September 14, 2021

Citation: Li Y, Xie K, Wang C, *et al.,* 2021, 3D Printing of Tricalcium Phosphate/Poly Lactic-co-glycolic Acid Scaffolds Loaded with Carfilzomib for Treating Critical-sized Rabbit Radial Bone Defects. *Int J Bioprint*, 7(4):405. http://doi.org/10.18063/ijb.v7i4.405

1. Introduction

To date, regeneration of long bone with critical-size defects induced by steroid-induced osteonecrosis, tumor resection, osteoporotic fractures, or accidental trauma is still challenging. Among various bone regeneration therapies, autologous bone transplantation is recognized as the gold standard[1,2]. However, its mass application is severely restricted due to insufficient donor sources. In the past decade, scaffold-based tissue engineering has gained increasing attention in treating bone defects[4-7]. In addition to the required biocompatibility, biodegradability and appropriate mechanical properties, capability of promoting osteogenesis and angiogenesis should also be imparted to the bone tissue engineering scaffolds[3].

Calcium phosphate has been widely used for the producing artificial protheses with a dense structure due to its high compositional similarity to bone apatite and high bioactivity[4]. Animal studies and clinical experiments have shown that calcium phosphates have excellent repair effects on bone regeneration[5-7]. To improve the repair capability of calcium phosphates, porous scaffolds made of calcium phosphate/biodegradable polyester composites which are structurally similar to native cancellous bone tissue have been developed[8]. The porous structure of scaffolds facilitates cell growth, migration, and transportation of nutrients and metabolites[9]. To further improve the osteogenic capability of bone tissue engineering scaffolds, growth factors and drugs related to osteogenesis and/or angiogenesis can be incorporated[10].

Additive manufacturing has gained increasing attention in making bone tissue engineering scaffolds as it is advantageous in producing scaffolds with customized shape, pore size, porosity, and interconnectivity[11]. Cryogenic 3D printing is a new type of additive manufacturing technology that uses polymeric water-in-oil emulsions as printing inks to deposit three-dimensional (3D) patterns below 0°C[12]. The emulsion inks immediately solidify when they contact the cryogenic substrate, allowing a layer-by-layer material deposition. After cryogenic 3D printing, as-printed 3D patterns are lyophilized to remove solvents to obtain stabilized scaffolds with a hierarchical structure[10].

The success of scaffold-based bone tissue engineering not only relies on the employment of advanced scaffolds but also depends on the use of newly discovered functional drugs. However, creation of new drug and its clinical approval cost a long time and a lot of money. Therefore, producing advanced scaffolds loaded with repositioned conventional drugs with effective osteogenesis capability, whose biosafety has been verified clinically, has gained increasing attention in the treatment of critical-sized defect in long bone. Carfilzomib (CFZ) is an approved clinical proteasome inhibitor with a much fewer side effects, replacing bortezomib in the treatment of multiple myeloma by inhibiting osteoclast activity and pathological bone destruction through the disruption of receptor activator for Nuclear factor kappa B [NF-κB] ligand (RANKL)-induced NF-κB signaling[13]. It is also reported that CFZ could induce increased alkaline phosphatase activity and upregulated expression of the osteogenic transcription factors such as osterix, osteopontin, and osteocalcin (OCN) through Wnt pathway by activating the β-catenin/T-cell factor (TCF) pathway[14-16].

The Wnt pathway is a complex signaling system involving the mutual regulation of multiple factors, and can interact with other signaling pathways and various cytokines. It is known that β-catenin protein in the Wnt pathway enters the nucleus and binds to TCF/lymphoid enhancer factor transcription factors to regulate the expression of genes related to cell proliferation, migration and differentiation, which are related to bone formation[17]. The Wnt pathway not only indirectly inhibits osteoclasts through osteoprotection in osteoblasts but can also directly regulate the function of osteoclasts by activating its own pathway[18,19]. Activation of the Wnt/β-catenin signaling is not only related to aging or directed differentiation of mesenchymal stem cells into osteoblasts[20], but also involved in the development, maturation, and function of osteoblasts[21].

To elucidate the combination effect of CFZ and 3D printed bony environment on the bone regeneration in long bone with defect and the underlying mechanism, in this study, a porous β-tricalcium phosphate/poly lactic-co-glycolic acid (TCP/PLGA) scaffold incorporated with CFZ was fabricated through cryogenic 3D printing. The morphological and physical properties of scaffolds and release behavior of CFZ were investigated. The positive effects of drug CFZ/TCP/PLGA scaffolds on the osteogenesis and angiogenesis and the inhibitory effect of CFZ on osteoclasts were studied *in vivo*. Significantly improved new bone formation and enhanced vascularization were observed in the regenerated tissue in radial defects of rabbits. This study suggests that the employment of 3D printed porous bone tissue engineering scaffolds incorporated with CFZ can effectively treat long bone defects by activating the Wnt/β-catenin signaling.

2. Materials and methods

2.1. Scaffold fabrication

The formulation of printing inks and the fabrication process of the 3D printed bone tissue engineering scaffolds (designated as "cytidine triphosphate [CTP]") are shown in **Figure 1**. The CTP material was prepared by in situ incorporation of CFZ in TCP/PLGA (TP) scaffolds using cryogenic 3D printing based on TCP/PLGA (TP) material. First, 3 g of PLGA (Shandong Medical Device Company,

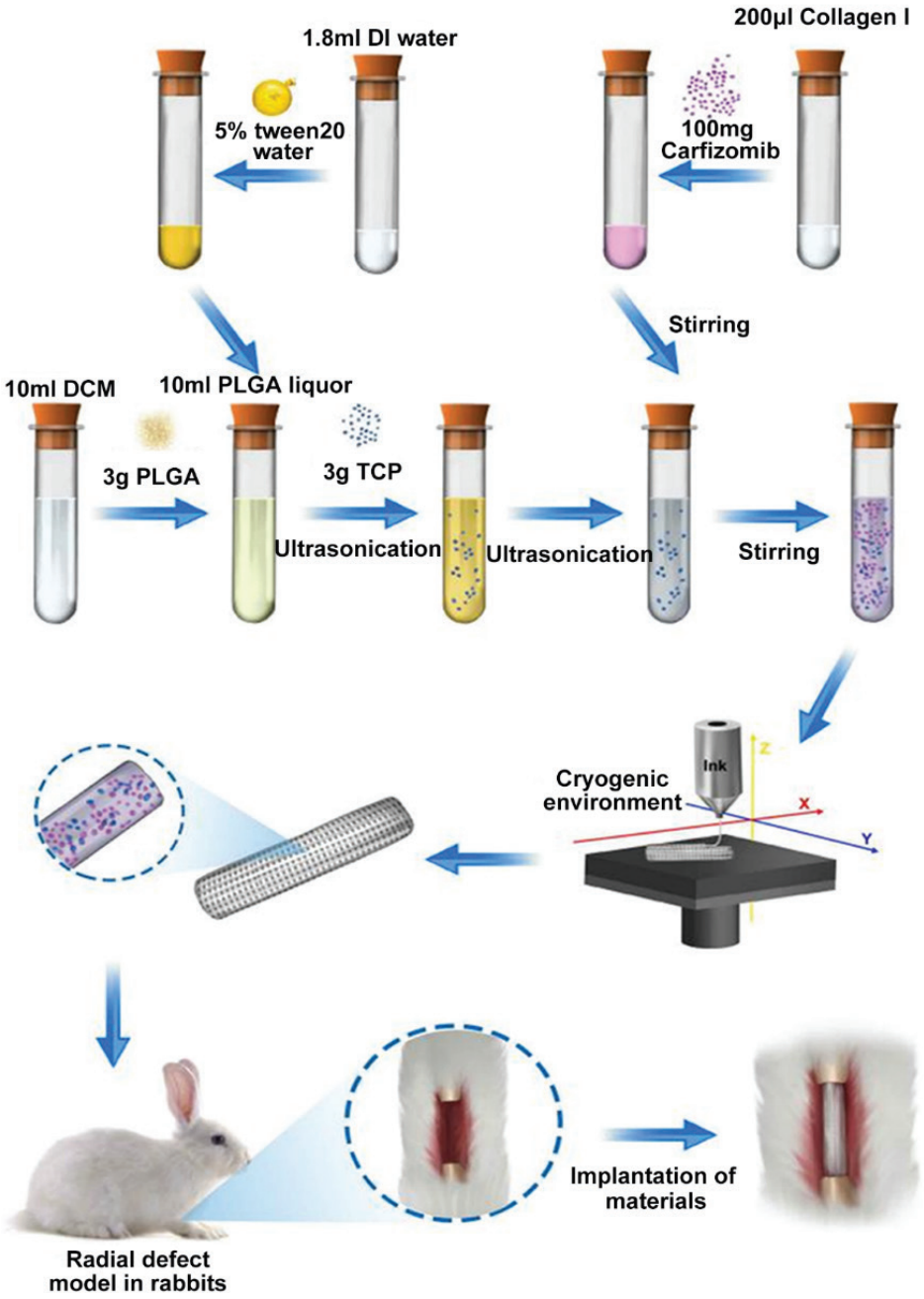

Figure 1. Schematic diagram depicting the fabrication of the 3D-printed β-tricalcium phosphate/poly lactic-co-glycolic acid carfilzomib-loaded scaffolds.

P.R. China) was dissolved in 10 mL of dichloromethane (DCM) and vortex-stirred for 15 min until the PLGA was fully dissolved. Then, 1.8 mL of deionized (DI) water and 50 μL of Tween 20 water were added to the PLGA to prepare 10 mL of PLGA organic solution. Afterward, 3 g of β-TCP powder mixture was mixed in the solution by ultrasonic vibration for 15 min to form TCP/DI water/PLGA/DCM composite emulsion inks (designated as "TP"). To load CFZ in TP inks, 100 mg of CFZ and 4.6 μL of NaOH (1 N, to neutralize the acidic collagen I solution) were dissolved in 200 μL of collagen I solution (9 mg/mL) at 4°C, and the CFZ/collagen I solution was homogeneously mixed with TP inks to obtain CFZ/TCP/PLGA/DCM emulsion ink (designated as "CTP"). The as-formulated CTP inks were added into a 20 mL syringe which was connected to a V-shaped plastic nozzle (inner diameter: 0.4 mm) and further loaded into a cryogenic 3D printer (Shenzhen Creality 3D Technology Co., Limited, P.R. China). Following the CAD file (a cylinder with a diameter of 4 mm and a height of 15 mm), porous 3D

cylindrical scaffolds were drawn (each layer consists of seven parallel struts, and struts in adjacent layers had a cross angle of 90°, Figure S1-A). The printing process is shown in Figure S1-B. The emulsion mixture was extruded by pushing the plunger of the syringe via an electromechanical screw, and the as-printed pattern was frozen in 2 s due to the existence of the cryogenic environment (−30°C). The printing speed is 6 mm/s and the feeding rate of the plunger was set as 0.008 mm/s. After the cryogenic 3D printing, the as-fabricated scaffolds were freeze-dried to remove water and DCM. Thus, a stable cylindrical bone tissue engineering scaffold with a diameter of 3 – 4 mm and a height of 15 mm was obtained.

2.2. Morphology observation and structural characterization analysis

The surface morphology was observed by scanning electron microscopy (SEM) (Gemini, Zeiss, Germany). Before SEM, a thin layer of gold was sprayed on the surface of the material to improve its electrical conductivity. The average pore size of the specimen was measured by SEM. On the basis of TP material, TCP/PLGA slow-release CFZ was prepared by cryogenic 3D printing to make CTP material. Micro-CT and SEM were used to evaluate the structure of the CTP.

2.3. Mechanical properties of the scaffold

The scaffolds were 15 mm thick, 3.4 mm wide, and 2.3 mm high. TP and CTP materials were tested by an electronic universal testing machine (SUNS, Shenzhen, China). The test and load-displacement curve were carried out at a speed of 1 mm/min and 40 s. Finally, the corresponding values of compressive strength, compression modulus, and compressive strain were obtained according to the GB/T 1041-92 calculation standard.

2.4. *In vitro* release of the scaffold

To study CFZ release *in vitro*, preweighed stent samples were placed in tubes containing phosphate-buffered saline (PBS) solution (0.02% sodium azide for CFZ test). The test tube was placed in an oscillating water bath at 37°C, the test solution was taken out at a predetermined interval, and the concentration of CFZ was determined using the CFZ Determination Kit (US Biological, USA) and the release time was determined.

2.5. Cell culture

Mouse mesenchymal stem cells C3H10T1/2 were cultured in Dulbecco's Modified Eagle Medium (DMEM) medium supplemented with 10% fetal bovine serum (FBS), 100 U/mL penicillin G, and 100 mg/mL streptomycin under standard conditions. To induce osteogenesis, this medium was added with 0.1 mM dexamethasone (Sigma-Aldrich, St. Louis, MO. USA), 100 μg/mL ascorbic acid (Sigma-Aldrich), and 10 mM β-glycerol phosphate (Sigma-Aldrich). RAW264.7 cell line (ATCC) was maintained in DMEM containing 10% FBS. The medium was changed every 2 days. For osteoclastic differentiation, cells were incubated with medium containing 50 ng/ml RANKL (R and D Systems, Minneapolis, MN, USA) for 7 days. In the control group and CFZ group, the cells were stimulated with dimethylsulfoxide (DMSO) and the extracts of scaffolds, respectively.

2.6. Western blot analysis

The cells were lysed in 2% sodium dodecyl sulfate (SDS), 2 M urea, 10% glycerol, 10 mM Tris-HCl (pH 6.8), 10 mM dithiothreitol, and 1 mM phenylmethylsulfonyl fluoride. Proteins were separated by 10% SDS-polyacrylamide gel electrophoresis. After electrophoresis, the proteins were transferred to the membrane by wet transfer (Bio-Rad Laboratories, Hercules, CA, USA). Each membrane was incubated with TBST (100 mM Tris-HCl pH 7.5, 150 mM NaCl, 0.05% Tween 20) and 5% non-fat blocking milk powder at room temperature for 1 h, and then incubated overnight with the primary antibody in a shaking bottle at 4°C. The membrane and HRB-conjugated secondary antibody were incubated at room temperature for 1 h. The membrane was then treated with enhanced chemiluminescence reagent (ECL Kit, Amersham Biosciences, Piscataway, NJ, USA), and the proteins were detected using chemiluminescence technology.

2.7. Gene expression and real-time polymerase chain reaction (PCR) analysis

The expression of osteogenesis genes, such as Alkaline Phosphatase (ALP), bone morphogenetic protein 2 (BMP2), collagen type I, Osteocalcin (OCN), transcription factor SP7 (Osterix), and Runt-related transcription factor 2 (Runx2) in C3H10T1/2 cells, and of osteoclastogenic genes, such as Cathepsin K (CTSK), Matrix metalloproteinase-9 (MMP9), c FBJ osteosarcoma oncogene (c-fos), Nuclear factor of activated T cells cytoplasmic 1 (NFATC1) in Raw264.7 cells cultured in different treatments was detected by PCR. Total RNA was extracted from the cells with Trizol reagent (Life Technologies, Carlsbad, CA, USA). The concentration of RNA was determined by a NanoDrop spectrophotometer (Thermo Fisher Scientific, USA). Primers for real time PCR (RT-PCR) are listed in **Table 1**.

2.8. Alizarin red S staining

C3H10T1/2 cells were seeded into 48-well plates (three wells per group). After osteogenic induction for 14 days, the cells were fixed in 4% paraformaldehyde, and then rinsed twice in PBS. Afterwards, they were stained at room temperature

Table 1. Primer sequences of osteogenic and osteoclastic genes

Genes	Primer sequences
ALP	Forward: 5'-CGG ATC CTG ACC AAA AAC C-3'
	Reverse: 5'-TCA TGA TGT CCG TGG TCA AT-3'
OCN	Forward: 5'-CAC CAT GAG GAC CCT CTC TC-3'
	Reverse: 5'-TGG ACA TGA AGG CTT TGT CA-3'
Osterix	Forward: 5'-TCT CCA TCT GCC TGA CTC CT-3'
	Reverse: 5'-AGC GTA TGG CTT CTT TGT GC-3'
Runx2	Forward: 5'-GAC TGT GGT TAC CGT CAT GGC-3'
	Reverse: 5'-ACT TGG TTT TTC ATA ACA GCG GA-3'
CTSK	Forward: 5'- CCA GGA AAT GAG CTT GAC AAA-3'
	Reverse: 5'- ATA ATT CTC AGT CAC ACA GTC CAC A -3'
MMP9	Forward:5'- CAC TCC CAC CCT GAG ATT TGT-3'
	Reverse: 5'- CCCC AGA GAC ATG ATG AAG TCA -3'
c-fos	Forward: 5'- TGT CTG TGG CTT CCC TTG AT -3'
	reverse: 5'- ATC AAA GGG CTC GGT CTT CA -3'
NFATc1	Forward:5'- CCG TTG CTT CCA GAA AAT AAC A -3'
	Reverse: 5'- TGT GGG ATG TGA ACT CGG AA -3'
GAPDH	Forward:5'-CAT GTA CGT TGC TAT CCA GGC-3'
	Reverse: 5'-CTC CTT AAT GTC ACG CAC GAT-3'

in 40 mM alizarin red S staining solution for 10 min, rinsed twice in PBS, and visualized under a light microscope.

2.9. Immunofluorescence analysis

For immunofluorescence analysis, cells were incubated first with primary antibodies and then with Alexa Fluor 594 donkey anti-mouse IgG1 (Life Technologies, Carlsbad, CA, USA) and Alexa Fluor 488 goat anti-mouse IgG2b (Life Technologies) secondary antibodies. Cells were washed 3 times in PBS, after which nuclei were counterstained with 4',6-diamidino-2-phenylindole (Life Technologies). Images were obtained on a confocal laser scanning microscope (Olympus, Tokyo, Japan).

2.10. Animal model and material implantation

Fifteen New Zealand white rabbits (2.5 ± 0.5 kg) were provided by the Scientific Experimental Center of Youjiang Medical University for Nationalities (YYFY-TYJ-20200225). The animal experiments were approved by the Research Ethics Committee of Youjiang Medical College for Nationalities. Pentobarbital sodium (20 mg/kg) with a volume fraction of 3% was injected through an ear vein, and ketamine was injected with 50% ketamine mg/kg through intramuscular injection for anesthesia. After successful anesthesia, the rabbit was fixed on the operating table in the prone position. The bilateral forelimbs were facing upward, and the rabbit hair of both forearms was removed. The operation area was disinfected with a tincture of iodine and alcohol, and laid with a sterile towel. The skin, subcutaneous tissue, and deep fascia were cut through to the middle and upper radial forearm, and the muscle space was separated to expose the radius. A section of the radius and periosteum at 2.5 – 3.0 cm below the radial head was cut off, together with the periosteum. The ulnar and radial interosseous membrane and the periosteum on both sides of the broken end were removed. The broken end of the defect was flattened as far as possible with a file. A syringe was filled with 50 mL normal saline and used to wash the bone debris and related congestion scab and bone marrow tissue in the bone marrow cavity. On the experimental side, the CTP material was implanted between the broken ends. Corresponding control groups (TP group, blank group) were set up. The muscle membrane and subcutaneous tissue were sutured with 4-0 absorbable sutures, and the skin incision was sutured with 0 braided suture to disinfect the wound. After the operation, the bilateral forelimbs were not fixed. Penicillin 40 kU (1.6 million units, QD) was immediately injected intramuscularly. Intramuscular injection of penicillin 40 kU/D was performed for 3 consecutive days after the operation. The animals were fed by the same feeder in separate cages. After the operation, the feeding condition of the animals, the appearance of the limbs on the operation side, the infection of the surgical incision, and the activity function were observed. At 12 weeks after the operation, the animals were killed and the original incision was opened to observe the formation of local callus and growth of the bone defect.

2.11. Micro-computed tomography (CT) scan and 3D reconstruction

At 8 and 12 weeks after implantation, the rabbits were sacrificed by injecting air into the auricular vein. Specimens of the radial defects were collected and fixed for 1 week in 10% formalin. Then, micro-CT (Scanco Medical, Bassersdorf, Zurich, Switzerland) with a spatial resolution of 12 μm and 55 kVp and 145 μA was used

to scan the radial defects in the rabbits. The regions of interest were selected and reconstructed. Then, 510 axial images were reconstructed into 3D images. In the bone tunnel, the residual scaffolds could be distinguished from the newly formed bone in the tunnel by setting different gray levels. The gray threshold from 40 hu to 60 hu represented the implanted composite scaffold, and the gray threshold from 80 to 255 represented new bone. The changes in stent volume after implantation were analyzed.

2.12. Microfil angiography and micro-CT imaging

After the New Zealand white rabbits had been anesthetized, their abdomen was fixed on the plate with the abdomen facing upward. The skin and muscle layers were cut along the midline of the abdomen. The xiphoid process was lifted, the diaphragm was cut open, and the heart was exposed. The heart was fixed with hemostatic forceps, a 23 G needle was inserted into the left ventricle, and the right auricle was cut with ophthalmic scissors. The perfusion pump was opened. The perfusion pump was irrigated with normal saline until no red liquid flowed out and was then changed to 4% paraformaldehyde. After the muscle tissue was fixed, 40 – 50 ml of mixed microfil liquid (solvent: solute = 4:5 and 1 – 2% coagulant) was infused. At the end of the perfusion, the small mesenteric vessels turned yellow. The rabbit carcass was kept in a 4°C refrigerator overnight. After the contrast medium was fixed, the rabbits' upper limbs were taken for micro-CT scanning to observe the vascular development.

2.13. Histology analysis

At 12 weeks, the rabbits were sacrificed by injecting air into the ear edge vein. The skin and muscle tissues were removed, and the radial specimens were obtained. The specimens were fixed in 4% PFA solution for 2 weeks and then decalcified with 10% EDTA solution for 4 – 6 weeks. The decalcification was continued until the needle could be easily inserted into the bone tissue. Gradient concentrations of ethanol solution were used for dehydration, and a xylene soak for 30 min was used to clear the tissue. This was repeated twice. The treated tissues were immersed in paraffin for 30 min, and the paraffin was replaced 3 times. After paraffin solidification, the embedded specimens were taken out and cut into 5-μm slices. They were then put in distilled water, pasted to a slide, and baked at 60°C overnight. The prepared paraffin sections were used for hematoxylin and eosin staining.

2.14. Statistical analysis

All quantitative data were obtained from four or five independent experiments. The results are expressed as the mean ± standard deviation. One-way analysis of variance (ANOVA) was used for statistical analysis, and the data are indicated with * if the probability is <0.05 ($P < 0.05$).

3. Results and discussion

3.1. Scaffold characterization, mechanical properties and drug release behavior

The morphology and structure of CTP scaffolds were evaluated by SEM. As shown in **Figure 2A-D**, both scaffolds had a porous structure in both the horizontal and vertical (cross-sectional) directions, and the interconnected gridded pores had a side length of 200 ± 50 μm. Compared to TP scaffolds, CTP scaffolds had a rougher strut surface on which a number of micropores and numerous TCP particles with a diameter around 200 nm can be seen **(Figure 2E** and **F)**. The mechanical properties of the TP and CTP scaffolds were measured through compression testing and the results are shown in **Table 2** and **Figure 2G** and **2H**. The compressive strengths of TP and CTP were 1.20 MPa and 1.34 MPa, respectively, which are in the low range of trabecular bone (1.3 – 4.4 MPa)[22], and hence is suitable for treating bone defects. The *in vitro* release behavior of CTP scaffold was also studied. As shown in **Figure 2I**, 55% level of released CFZ was observed on day 5, and the release profile achieved a plateau after 10 days of incubation. The survival rate of C3H10T1/2 cultured on the TP and CTP scaffolds for 3 days (as shown in **Figure 2J**) was more than 90%, indicating that the TP and CTP scaffolds were a biocompatible platform for C3H10T1/2 culture.

3.2. CTP scaffolds promote osteogenic differentiation of C3H10T1/2 cells

To analyze the effect of CTP scaffold on osteogenesis, we treated the mouse mesenchymal cells line C3H10T1/2 with osteogenic media supplemented with extracts of the scaffold. **Figure 3A** shows the mRNA expression of the osteogenic genes in C3H10T1/2 cells stimulated with control or CFZ for 7 days. It was seen that the expression of osteogenic genes, including *ALP*, *BMP2*, *Col1α1*, *OCN*, *Osterix,* and *Runx2*, was all upregulated in CFZ group compared with control group. With Western blot analysis, we confirmed that the protein level of OCN, Col1α1, and Runx2 was increased, and the expression of *Runx2* and *Col1α1* was more pronounced in the CFZ group **(Figure 3B)**, which were accordant with the

Table 2. Compression mechanical results of TP and CTP scaffolds

Scaffold	Young modulus (E)	Ultimate tensile strength (UTS)	Strain
TP	31.52	1.20MPa	9.69%
CTP	33.13	1.34MPa	11.90%

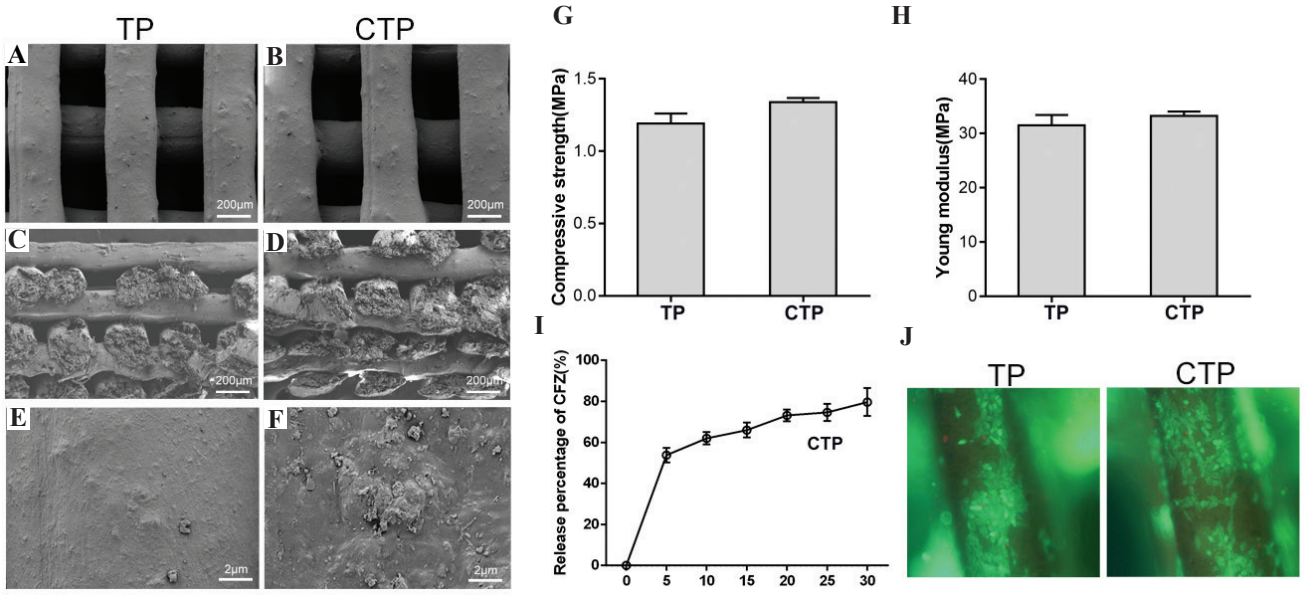

Figure 2. Fabrication of a 3D-printed β-tricalcium phosphate/poly lactic-co-glycolic acid scaffold loaded with carfilzomib (CFZ). (A-F) Scanning electron microscopy micrographs of different scaffolds at different magnification. (G) Compressive strengths of cytidine triphosphate (CTP) scaffolds and TP controls. (H) Young modulus of the CTP scaffolds and TP controls. (I) Release behavior of CFZ from CTP scaffolds in a 30-day test period. (J) Cell viability after seeding C3H10T1/2 in the scaffolds for 3 days.

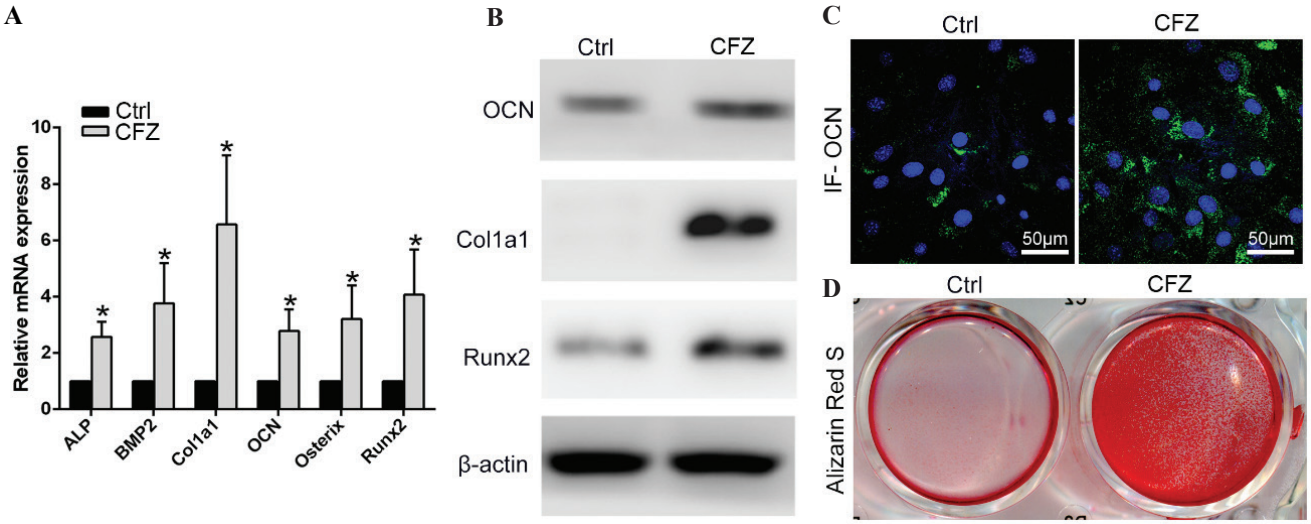

Figure 3. Cytidine triphosphate (CTP) scaffolds promote osteogenic differentiation in C3H10T1/2 mesenchymal cells. (A) mRNA expression of osteogenic genes in C3H10T1/2 cells stimulated with osteogenic medium supplemented with (carfilzomib [CFZ] group) or without (control group) extracts of the CTP scaffold for 7 days. (B) Western blot results of osteogenic proteins in C3H10T1/2 cells from control and CFZ group. (C) Immunofluorescence staining of osteocalcin in C3H10T1/2 cells from control and CFZ group. (D) Alizarin red S staining of C3H10T1/2 cells stimulated with osteogenic medium supplemented with (CFZ group) or without (control group) extracts of the CTP scaffold for 14 days. Scale bar = 50 μm. *$P < 0.05$.

mRNA expression levels. In addition, we performed immunofluorescence staining of OCN in C3H10T1/2 cells from control and CFZ groups. As shown in **Figure 3C,** OCN expression in CFZ group was remarkably enhanced compared to control group. And within 14 days, alizarin red staining confirmed enhanced mineralization of the extracellular matrix in CFZ group **(Figure 3D)**. Therefore, these data suggest that CTP scaffolds have good osteogenic capabilities *in vitro*.

3.3. CTP scaffolds inhibit osteoclast formation *in vitro*

The role of CFZ in osteoclast activity has been mentioned in the previous studies. In this study, we also investigated

the effect of CTP scaffolds on osteoclast formation in cultured cells. The mouse leukemic monocyte cell line RAW264.7 was stimulated with RANKL and supplemented with or without extracts of the scaffold. As shown in **Figure 4A,** mRNA expression of osteoclast differentiation marker genes (*Ctsk* and *Mmp9*), key transcription factors (*c-fos* and *NFATc1*), and osteoclast fusion-related genes (*β3-integrin*) were all dramatically downregulated in CFZ group compared to the control group. We ascertained the decreased protein level of CTSK, NFATc1, and MMP9 in CFZ group with Western blot analysis **(Figure 4B)**. RANKL induces macrophages to differentiate into osteoclast through the induction of multiple regulatory transcription factors, such as NF-κB and NFATc1. Our results suggested that CFZ had an inhibitory effect on osteoclastogenesis through the RANKL-related pathway. To better understand the potential role of CTP scaffolds on actin ring formation in osteoclasts, we conducted immunofluorescence staining of phalloidine (F-actin) and CTSK in raw264.7 cells. Our data showed that in control group, CTSK-positive cells, multinucleated osteoclasts, and well-polarized F-actin ring were observed, while all these were inhibited in cells of CFZ group (**Figure 4C**)**.** These data indicate that CTP scaffolds inhibit osteoclast formation partially through RANKL-related pathway and destroy the actin ring formation, which was consistent with the finding of a previous study[15].

3.4. CTP scaffolds activate Wnt/β-catenin signaling

To determine the underlying mechanism of CTP scaffolds on osteogenesis and osteoclast formation, we analyzed the effect of CTP scaffolds on the Wnt/β-catenin signaling in C3H10T1/2 cells. Western blot analysis indicated that the total expression of β-catenin was slightly elevated while the increased expression of active β-catenin was more pronounced in CFZ group compared to control group (**Figure 5A**). TOP/FOP-Flash luciferase reporter assay also confirmed the activity of Wnt/β-catenin signaling was significantly upregulated in CFZ group (**Figure 5B**). Next, we detected the expression of β-catenin in C3H10T1/2 cells with immunofluorescence staining. As shown in **Figure 5C**, cells in CFZ group exhibited enhanced total and nuclear expressions of β-catenin in comparison with control. All these results indicated that CTP scaffolds may enhance the activity of the Wnt/β-catenin signaling *in vitro*. We speculated that the effect of CFZ on osteogenesis and osteoclast formation may be mediated through the activation of Wnt/β-catenin signaling.

3.5. CTP scaffolds promote bone regeneration in a rabbit long bone defect model

Next, we analyzed the effect of CTP scaffold in a rabbit long bone (radius) defect model. After surgery and stent implantation **(Figure 6A)**, the specimens of each group were taken out after 12 weeks of cage feeding. With micro-CT scan, we noticed that the degree of bone formation in the CTP scaffolds group was significantly higher than in the TP group and the control group (**Figure 6B**). **Figure 6C** and **D** shows the bone volume/total volume (BV/TV) ratio and bone mineral density of different groups. It can be seen that CTP scaffolds induced the highest level of BV/TV ratio and bone mineral density value. These data suggest that the sustained release of CFZ significantly improved bone mineralization. In the process of bone regeneration, blood vessel formation is essential because vascularization can also facilitate

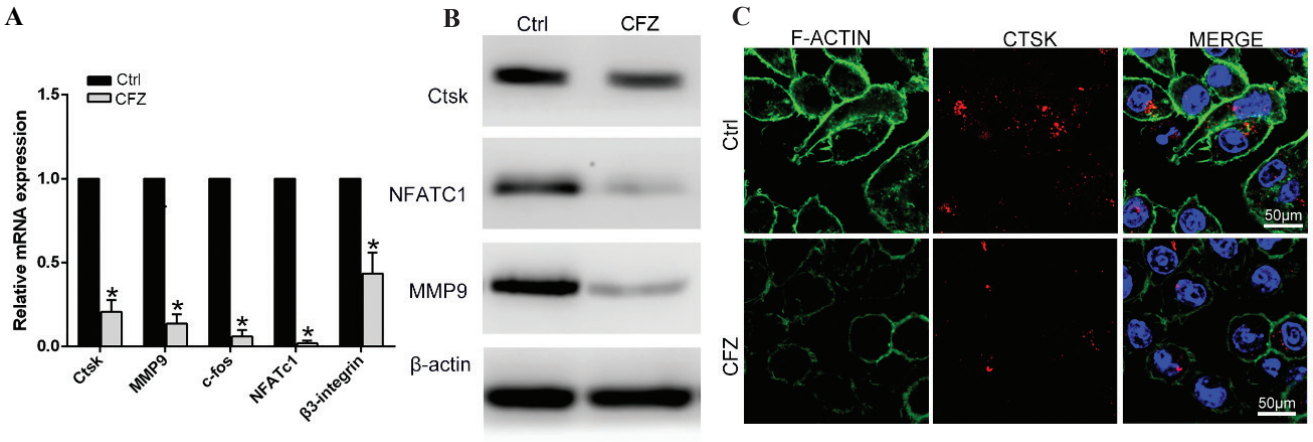

Figure 4. Cytidine triphosphate (CTP) scaffolds inhibit osteoclast formation in RAW264.7 cells. (A) mRNA expression of osteoclast formation genes in RAW264.7 cells stimulated with RANKL and supplemented with (carfilzomib [CFZ] group) or without (control group) extracts of CTP scaffold for 7 days. (B) Western blot results of Ctsk, MMP9 and NFATC1 in raw264.7 cells from control and CFZ group. (C) Immunofluorescence staining of F-actin and CTSK in raw264.7 cells stimulated with RANKL and supplemented with (CFZ group) or without (control group) extracts of CTP scaffold for 14 days. Scale bar = 50 μm. *$P < 0.05$.

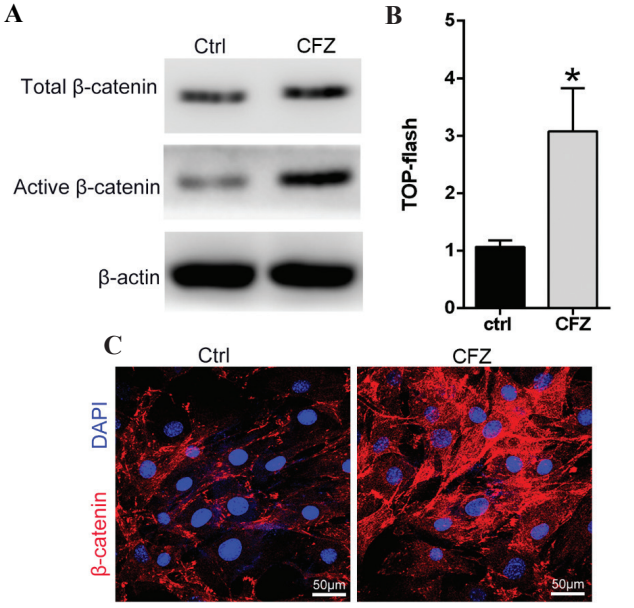

Figure 5. Cytidine triphosphate (CTP) scaffolds activate Wnt/β-catenin signaling. (A) Western blot results of β-catenin in C3H10T1/2 cells cultured with medium supplemented with (carfilzomib [CFZ] group) or without (control group) extracts of the CTP scaffold. (B) TOP/FOP-Flash luciferase reporter assay was used to analyze the effect of CTP scaffolds on the activity of Wnt/β-catenin signaling in C3H10T1/2 cells. (C) Immunofluorescence staining of β-catenin in C3H10T1/2 cells from control and CFZ group. Scale bar = 50 μm. **P* < 0.05.

bone formation. The 3D image of the neovascularization structure in the scaffold area is shown in **Figure 6E**. Neovascularization was significantly enhanced in CTP stents in CFZ group compared to the control group, which was at least 2 times more than TP stents, and at least 4 times more than the blank group. Thus, our data indicated that CTP scaffolds can significantly promote bone regeneration and neovascularization by showing significantly improved vessel length and vessel density **(Figure 6F** and **G)**.

Subsequently, animals were sacrificed and we performed H and E staining to examine the formation of bone in orthotropic segmental defects of each group. As shown in **Figure 7A**, CTP scaffolds showed a better effect in new bone formation and blood vessel formation compared to others, while the control and TP groups showed more fibrous tissue formation than mature bones. Next, we labeled the osteoclasts through immunofluorescence staining of CTSK in bone samples from each group. Compared to the other two groups, CTP scaffolds group showed a reduced level of CTSK on the surface of the trabecular bone (**Figure 7B** and **E**), indicating that CTP scaffolds inhibited osteoclasts formation *in vivo*. We also labeled the vessel with immunofluorescence staining of CD31 in bone sections from all groups, and as expected, the number of vessels around the new formation bone in CTP group was more than that in other two

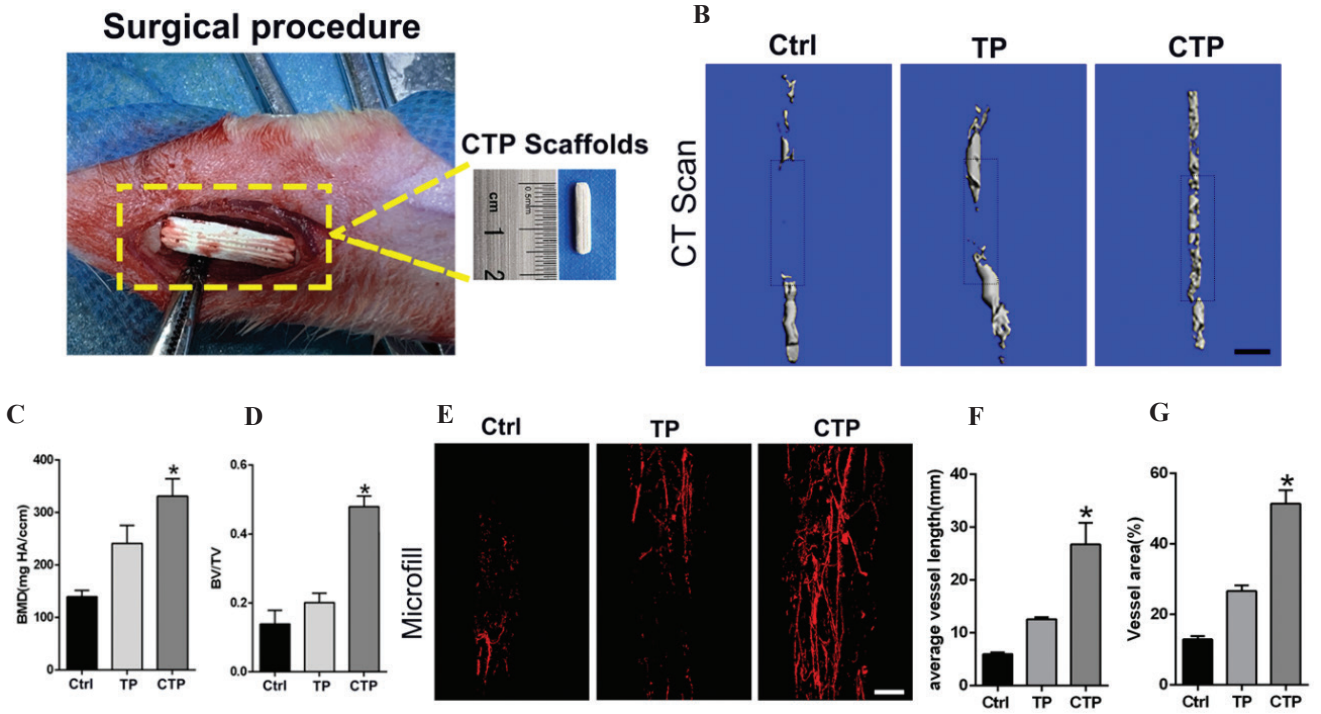

Figure 6. Imaging results show cytidine triphosphate scaffolds promote bone regeneration in a rabbit long bone defect model. (A) Surgical procedure in rabbits with the scaffolds. (B) Micro-CT scan images of the defect area at 12 weeks post-surgery. (C) Bone mineral density of regenerated bone tissue. (D) BV/TV ratio of regenerated tissue. (E) Microfil angiography and micro-CT imaging results of the experimental animals. (F) Quantification of average vessel length and vessel area (G) of the experimental animals **P* < 0.05.

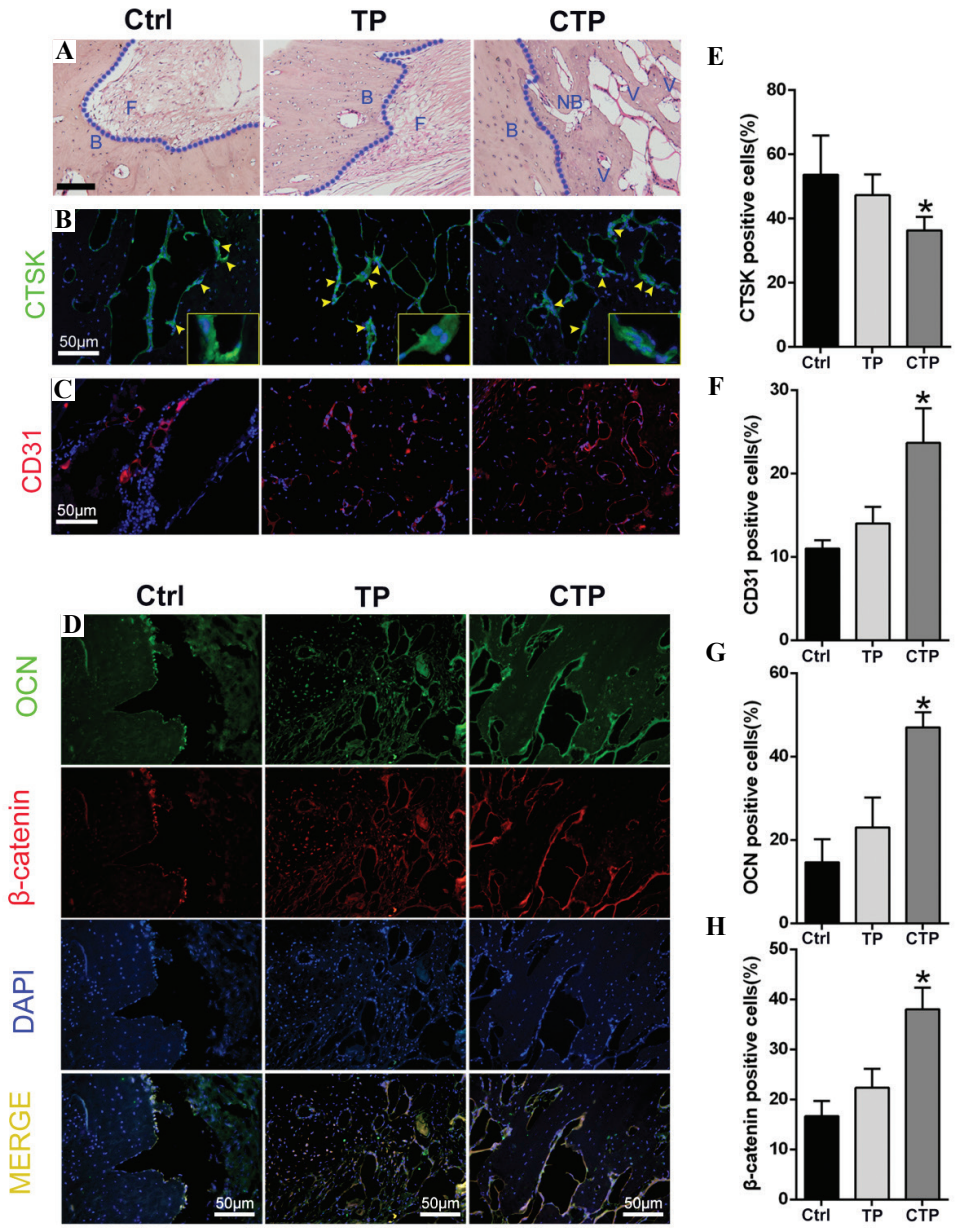

Figure 7. Histological results show that cytidine triphosphate scaffolds promote bone regeneration in a rabbit long bone defect model. (A) H&E staining of the defect area at 12 weeks post-surgery. B: bone, F: Fibrous tissue, NB: New bone; V: Vessel). (B and E) IF analysis and quantification of CTSK in bone sections from different groups. (C and F) Immunofluorescence analysis and quantification of CD31 in bone sections from all groups. (D, G, and H) Immunofluorescence analysis and quantification of OCN and β-catenin in bone sections from different groups. Scale bar = 50 μm. *$P < 0.05$.

groups (**Figure 7C and F**), indicating that the released CFZ promoted angiogenesis in the defected area. Further, expression of ontogenetic marker OCN and β-catenin was detected. We noticed that OCN and β-catenin co-localized in the cytoplasm and nucleus. In the CTP scaffolds, the expression of both OCN and β-catenin was higher than in other groups, suggesting that CTP scaffolds promoted osteogenesis and possibly via the activation of the β-catenin signaling (**Figure 7D**, **G**, and **H**).

Treatment for large bone defects resulting from trauma, tumor, or other diseases is still a major clinical challenge. Autologous bone or autograft is still the most effective therapeutic approaches for bone regeneration in large bone defect[23]. In recent years, bone graft scaffolds combined with various growth factors, such as BMPs, mesenchymal stem cells, and other agents, have been used in the repair of bone defects[24]. The most ideal bone graft scaffold should be biocompatible, osteogenic, and

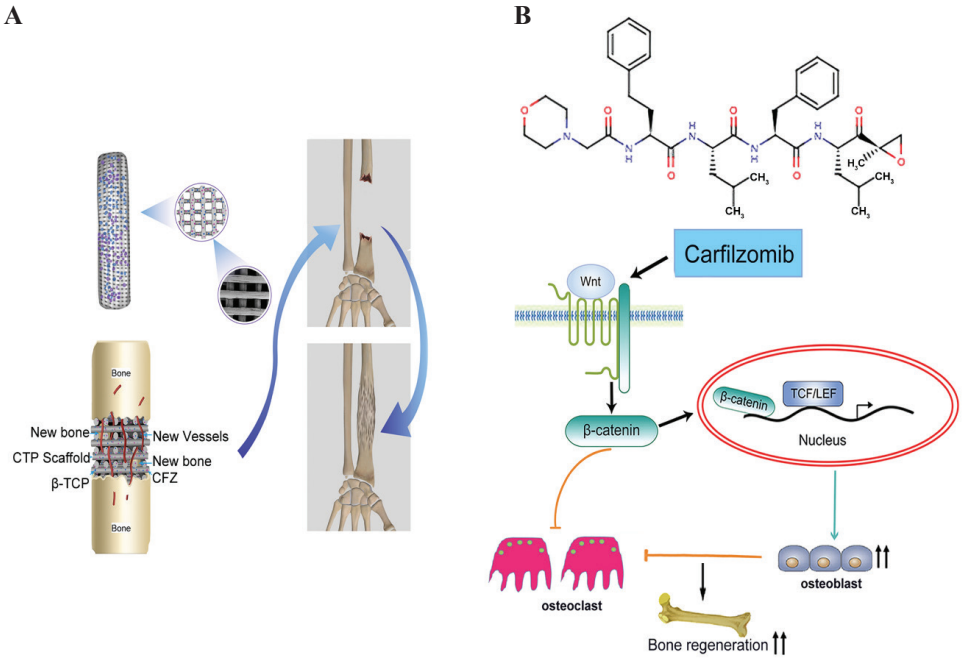

Figure 8. Schematic diagram of cytidine triphosphate (CTP) scaffolds promoting bone regeneration via activating Wnt/β-catenin pathway. (A) Schematic diagram of the preparation process of the CTP scaffold and its effect on angiogenesis and osteogenesis in the bone defect. (B) Chemical structure of carfilzomib and mechanism of carfilzomib on the canonical Wnt/β-catenin signaling.

angiogenic and have mechanical properties similar to those of bone at the implant site[25].

CFZ, an clinically approved proteasome inhibitor, is used to replace bortezomib to treat multiple myeloma, due to fewer side effects it causes[26]. The previous studies had reported the effect of CFZ in inhibiting osteoclasts formation and bone resorption, while enhancing osteogenic differentiation and matrix mineralization *in vitro*[15]. In our study, with sustained release of CFZ from CTP scaffolds, we confirmed the promotion of osteogenesis in cultured mouse mesenchymal cells and inhibition of osteoclastogenesis in mouse leukemic monocyte cell line. The canonical Wnt/β-catenin pathway has been found to be tightly linked to bone formation. Herein, after being treated with CTP scaffolds, the mesenchymal cells exhibited an increased expression of active β-catenin, and we noticed that β-catenin was translocated into the nucleus. Activation of canonical WNT/β-catenin signaling not only promotes differentiation of osteoblasts and bone production but also suppresses RANKL expression to inhibit osteoclasts formation[27]. Thus, we speculated that the effect of CFZ on osteogenesis and osteoclastogenesis may be mediated through activation of the WNT/β-catenin signaling.

During the progression of bone defect repair, osteoclast precursors are attracted from the invading blood vessels that are adjacent to the newly formed bone trabeculae[28]. The new bone tissue is continuously remodeled through the balancing activities of bone-forming osteoblasts and of bone-resorbing osteoclasts[29]. Since the CTP scaffolds showed good biomechanical properties and biocompatibility, we consider that the CTP scaffolds could be suitable for bone regeneration. In *in vivo* study, the CTP scaffolds-treated animals showed increased osteogenesis, decreased osteoclastogenesis, and notably improved bone formation. It was interesting to note that the vascularization was also enhanced in CTP-treated group. Osteogenesis and angiogenesis are two closely related processes in bone regeneration; the newly formed vessels transport nutrient to the cells and metabolic wastes away from the cells, thereby improving bone formation[30]. In summary, CTP scaffolds promoted osteogenesis, inhibited osteoclastogenesis through activation of WNT/β-catenin signaling, and also enhanced angiogenesis, thus improving bone regeneration in large bone defect (**Figure 8A** and **B**).

4. Conclusions

In this study, a porous CTP scaffold was generated by cryogenic 3D printing. The sustained release of CFZ from CTP scaffolds led to the induction of osteoblastic differentiation and inhibition of osteoclast formation *in vitro*, which may be mediated by an underlying mechanism where the CFZ activates the Wnt/β-catenin signaling. In the treatment of rabbit radius bone defects, CTP scaffolds improved new bone formation and promoted the growth of new blood vessels in the regenerated tissues. Overall, this study provides a theoretical basis for

CFZ-incorporated scaffolds, which are produced by 3D printing, in promoting bone regeneration in critical-sized bone defects.

Acknowledgments

This work was supported by Guangxi Science and Technology Program (2018GXNSFAA294116, 2018GXNSFAA138074,2018GXNSAA294091), Guangxi key R & D Project (Guike AB18050008), Scientific Research Project of High-level talents in the affiliated Hospital of Youjiang Medical College for nationalities (R20196301, R20196306), High-level Innovation team and Outstanding Scholars Program of Colleges and Universities in Guangxi: innovative team of basic and Clinical Comprehensive Research on Bone and Joint degenerative Diseases.

Conflicts of interest

The authors have no conflict of interest to declare.

Author contributions

K L., J L. and YJ T. conceived the project. Y L. KG X. and C W. conducted the scaffold fabrication, characterization. CL Y., GF D., GG H. and K H. conducted the *in vitro* release/degradation test and in vitro cell culture. F L., CC Z., SJ D. and J C. conducted the *in vivo* experiments in rat cranial defects and analyzed the related data. QY L., J L. and LQ W. contributed to the writing of the manuscript.

References

1. Sharif F, Ur Rehman I, Muhammad N, *et al*., 2016, Dental Materials for Cleft Palate Repair. *Mater Sci Eng C Mater Biol Appl*, 61:1018–28. https://doi.org/10.1016/j.msec.2015.12.019
2. Marx RE, 2007, Bone and Bone Graft Healing. *Oral Maxillofac Surg Clin North Am*, 19:455–66.
3. Agarwal R, García AJ, 2015, Biomaterial Strategies for Engineering Implants for Enhanced Osseointegration and Bone Repair. *Adv Drug Deliv Rev*, 94:53–62. https://doi.org/10.1016/j.addr.2015.03.013
4. Pilliar RM, Filiaggi MJ, Wells JD, *et al*., 2001, Porous Calcium Polyphosphate Scaffolds for Bone Substitute Applications-*In Vitro* Characterization. *Biomaterials*, 22:963–72. https://doi.org/10.1016/s0142-9612(00)00261-1
5. Lai Y, Li Y, Cao H, *et al*., 2019, Osteogenic Magnesium Incorporated into PLGA/TCP Porous Scaffold by 3D Printing for Repairing Challenging Bone Defect. *Biomaterials*, 197:207–19. https://doi.org/10.1016/j.biomaterials.2019.01.013
6. Lee JY, Son SJ, Son JS, *et al*., 2016, Bone-Healing Capacity of PCL/PLGA/Duck Beak Scaffold in Critical Bone Defects in a Rabbit Model. *Biomed Res Int*, 2016:2136215. https://doi.org/10.1155/2016/2136215
7. Walsh WR, Vizesi F, Michael D, *et al*., 2008, Bruceβ-TCP Bone Graft Substitutes in a Bilateral Rabbit Tibial Defect Model. *Biomaterials*, 29:266–71. https://doi.org/10.1016/j.biomaterials.2007.09.035
8. Huang J, Liu W, Liang Y, *et al*., 2018, Preparation and Biocompatibility of Diphasic Magnetic Nanocomposite Scaffold. *Mater Sci Eng C Mater Biol Appl*, 87:70–7.
9. Ji C, Annabi N, Khademhosseini A, *et al*., 2011, Fabrication of Porous Chitosan Scaffolds for Soft Tissue Engineering using Dense Gas Co_2. *Acta Biomater*, 7:1653–64. https://doi.org/10.1016/j.actbio.2010.11.043
10. Hartgerink JD, Beniash E, Stupp SI, 2002, Peptide-Amphiphile NanofibersA Versatile Scaffold for the Preparation of Self-Assembling Materials. *Proc Natl Acad Sci USA*, 99:5133–8. https://doi.org/10.1073/pnas.072699999
11. Green JD, Tollemar V, Dougherty M, *et al*., 2015, Multifaceted Signaling Regulators of ChondrogenesisImplications in Cartilage Regeneration and Tissue engineering. *Genes Dis*, 2:307–27.
12. Gaasbeek RD, Toonen HG, van Heerwaarden RJ, *et al*., 2005, Mechanism of Bone Incorporation of β-TCP Bone Substitute in Open Wedge Tibial Osteotomy in Patients. *Biomaterials*, 26:6713–9. https://doi.org/10.1016/j.biomaterials.2005.04.056
13. Michalicka M, Boisjoli G, Jahan S, *et al*., 2017, Human Bone Marrow Mesenchymal Stromal Cell-Derived Osteoblasts Promote the Expansion of Hematopoietic Progenitors Through Beta-Catenin and Notch Signaling Pathways. *Stem Cells Dev*, 26:1735–48. https://doi.org/10.1089/scd.2017.0133
14. Zhang C, Hu B, Chen Y, *et al*., 2013, Characterization of the Molecular Mechanism of the Bone-Anabolic Activity of Carfilzomib in Multiple Myeloma. *PLoS One*, 8:e74191. https://doi.org/10.1371/journal.pone.0074191
15. Hurchla MA, Garcia-Gomez A, Hornick MC, *et al*., 2012, The Epoxyketone-Based Proteasome Inhibitors Carfilzomib and Orally Bioavailable Oprozomib Have Anti-Resorptive and Bone-Anabolic Activity in Addition to Anti-Myeloma Effects. *Leukemia*, 27:430–40. https://doi.org/10.1038/leu.2012.183
16. Yang Y, Blair HC, Shapiro IM, *et al*., 2015, The Proteasome Inhibitor Carfilzomib Suppresses Parathyroid Hormone-induced Osteoclastogenesis through a RANKL-Mediated

Signaling Pathway. *J Biol Chem*, 290:16918–28. https://doi.org/10.1074/jbc.m115.663963

17. Maeda K, Kobayashi Y, Koide M, *et al*., 2019, The Regulation of Bone Metabolism and Disorders by WNT Signaling. *Int J Mol Sci*, 20:5525.
18. Wei W, Zeve D, Suh JM, *et al*., 2011, Biphasic and Dosage-Dependent Regulation of Osteoclastogenesis by β-Catenin. *Mol Cell Biol*, 31:4706–19. https://doi.org/10.1128/mcb.05980-11
19. Coffin JD, Homer-Bouthiette C, Hurley MM, *et al*., 2018, Fibroblast Growth Factor 2 and Its Receptors in Bone Biology and Disease. *J Endocr Soc*, 2:657–71. https://doi.org/10.1210/js.2018-00105
20. Zhou H, Mak W, Zheng Y, *et al*., 2008, Osteoblasts Directly Control Lineage Commitment of Mesenchymal Progenitor Cells through Wnt Signaling. *J Biol Chem*, 283:1936–45. https://doi.org/10.1074/jbc.m702687200
21. Barbosa MA, Yao D, Xie XH, *et al*., 2012, Icaritin, an Exogenous Phytomolecule, Enhances Osteogenesis but Not Angiogenesis-An *In Vitro* Efficacy Study. *PLoS One*, 7:e41264. https://doi.org/10.1371/journal.pone.0041264
22. Guzzo CM, Nychka JA, 2020, Bone 'Spackling' Paste: Mechanical Properties and *In Vitro* Response of a Porous Ceramic Composite Bone Tissue Scaffold. *J Mech Behav Biomed Mater*, 112:103958. https://doi.org/10.1016/j.jmbbm.2020.103958
23. Roddy E, DeBaun MR, Daoud-Gray A, *et al*., 2017, Treatment of Critical-Sized Bone Defectsclinical and Tissue Engineering Perspectives. *Eur J Orthop Surg Traumatol*, 28:351–62. https://doi.org/10.1007/s00590-017-2063-0
24. Ho-Shui-Ling A, Bolander J, Rustom LE, *et al*., 2018, Bone Regeneration Strategies: Engineered Scaffolds, Bioactive Molecules and Stem Cells Current Stage and Future Perspectives. *Biomaterials*, 180:143–62. https://doi.org/10.1016/j.biomaterials.2018.07.017
25. Polo-Corrales L, Latorre-Esteves M, Ramirez-Vick JE, 2014, Scaffold Design for Bone Regeneration. *J Nanosci Nanotechnol*, 14:15–56. https://doi.org/10.1166/jnn.2014.9127
26. McBride A, Klaus JO, Stockerl-Goldstein K, 2015, Carfilzomib: A Second-Generation Proteasome Inhibitor for the Treatment of Multiple Myeloma. *Am J Health Syst Pharm*, 72:353–60. https://doi.org/10.2146/ajhp130281
27. Glass DA, Bialek P, Ahn JD, *et al*., 2005, Canonical WNT Signaling in Differentiated Osteoblasts Controls Osteoclast Differentiation. *Dev Cell*, 8:751–64. https://doi.org/10.1016/j.devcel.2005.02.017
28. Wang Y, Li M, Li P, *et al*., 2019, Progress and Applications of Polyphosphate in Bone and Cartilage Regeneration. *Biomed Res Int*, 2019:5141204.
29. Hadjidakis DJ, Androulakis II, 2006, Bone Remodeling. *Ann N Y Acad Sci*, 1092:385–96.
30. Grosso A, Burger MG, Lunger A, *et al*., 2017, It Takes Two to Tango: Coupling of Angiogenesis and Osteogenesis for Bone Regeneration. *Front Bioeng Biotechnol*, 5:68. https://doi.org/10.3389/fbioe.2017.00068